Title

Scanner Design Considerations for Long Axial Field-of-View PET Systems

Journal

PET Clinics, 16(1)

ISSN

1556-8598

Authors

Daube-Witherspoon, Margaret E
Cherry, Simon R

Publication Date

2021

DOI

10.1016/j.cpet.2020.09.003

Peer reviewed

HHS Public Access

Author manuscript

PET Clin. Author manuscript; available in PMC 2022 January 01.

Published in final edited form as:

PET Clin. 2021 January ; 16(1): 25–39. doi:10.1016/j.cpet.2020.09.003.

Scanner design considerations for long axial field-of-view PET systems

Margaret E. Daube-Witherspoon, Ph.D. [Senior Research Investigator],
Department of Radiology, University of Pennsylvania, 3620 Hamilton Walk, Rm. 156H, Philadelphia, PA 19104

Simon R. Cherry, Ph.D. [Professor]
Department of Biomedical Engineering, University of California, Davis, 451 Health Sciences Drive, Davis, CA 95616

Keywords

Long axial FOV; scanner design; time-of-flight

1. Introduction

PET scanner designs have changed markedly over the past three decades with resulting dramatic improvements in image quality. Many of these advances in scanner technology directly impacted the design of recently developed long (≥70 cm) axial field-of-view (AFOV) PET scanners. In this chapter, we will discuss aspects of scanner design of long AFOV systems and how these choices affect system performance.

1.1 3D acquisition

With a few exceptions[1], most scanners built prior to the early 1990s had lead septa between the detector rings that restricted the contributions of random coincidences and scattered photons (within the object) but also resulted in low geometric sensitivity and long scan times, since only true coincidence events emitted within a series of two-dimensional slices could be detected. Removing the septa and operating as a fully three-dimensional (3D) system led to a 3–5x increase in the probability of detection of true coincidences (sensitivity) by detecting the oblique lines of response (LORs)[2]. However, with this sensitivity gain came a significant increase in detected random and scattered coincidences that required careful attention to their correction. All current-generation PET scanners operate in 3D with accurate corrections.

Corresponding author: daubewit@pennmedicine.upenn.edu.

Disclosure Statement: Dr. Daube-Witherspoon has sponsored research agreements with Siemens Healthcare and Philips Medical Systems. Dr. Cherry has sponsored research agreements with United Imaging Healthcare and Canon Medical Research USA. The University of California, Davis has a revenue sharing agreement with United Imaging Healthcare.

1.2 Time-of-flight (TOF) information

The measurement of the difference in arrival times (time-of-flight, TOF) of the two annihilation photons at the detectors and the incorporation of this information into the reconstruction as a means to reduce image noise was first proposed in the early 1980s[3]. Incorporating TOF information into the reconstruction improves the signal-to-noise properties of the image by restricting the back-projection of each event to the location of most probable annihilation based on the TOF difference, rather than assuming uniform probability along the LOR[4,5]. TOF information effectively enhances the sensitivity of the scanner by improving the signal-to-noise ratio of lesions. The scintillator crystals used at that time in PET scanners (bismuth germanate, BGO, and sodium iodide, NaI(Tl)) did not have adequate timing resolution to be useful in these early TOF systems. Instead, available fast scintillators such as BaF_2 and CsF were used[6–8]. However, these scintillators have reduced stopping power and light output, so the early TOF-PET systems had overall lower sensitivity and worse spatial and energy resolutions than nonTOF scanners at the time.

1.3 Scintillators and photomultipliers

The introduction of cerium-doped lutetium-based scintillators, such as lutetium oxyorthosilicate (LSO)[9] or lutetium-yttrium oxyorthosilicate (LYSO), allowed for better TOF resolution due to their faster decay constant (40 ns, compared to 300 ns for BGO), in addition to a high stopping efficiency that is close to that of BGO. The lutetium-based scintillators cost more to produce than BGO, but starting in the mid-2000s, fully-3D TOF-PET scanners based on LSO and LYSO were commercialized with TOF resolutions of 450–600 ps[10,11]. These systems used arrays of small crystals coupled to large (25–39 mm diameter) photomultipliers (PMTs) that convert the scintillation light into an electrical signal. More recently, TOF resolutions of 215–250 ps have been achieved when small crystals are coupled to another advancement in PET technology, silicon photomultipliers (SiPMs)[12–14]. SiPMs are more compact than PMTs and some designs use one-to-one coupling of crystals to SiPMs, thereby simplifying the calculation of event positions and reducing light losses that result from light sharing across photodetectors[15]. The vast majority of new commercial PET scanners for human use today use Lu-based scintillators read out by SiPM photodetectors although many PMT-based systems are still in clinical use.

1.4 State-of-the-art of PET systems for whole-body imaging

Most commercial PET systems are whole-body devices, with a ring diameter of 75–90 cm and an intended application of static [^{18}F]-fluorodeoxyglucose (FDG) imaging in oncology. The AFOV ranges from 16–30 cm, and patients are usually scanned in ~8–10 overlapping bed positions to cover the organs of interest (head-to-thighs for most oncology patients) in 10–20 min with a dose of 370–555 MBq of FDG. For dynamic imaging to capture the temporal behavior of radiotracer delivery, uptake, and clearance, patients are typically imaged in a single bed position over the heart for the first few min to capture the blood input function and then either moved to image a single bed position with good temporal sampling or cycled through the scanner to capture more distant lesions with coarse temporal sampling[16,17].

Table 1 summarizes the current-generation commercial SiPM-based PET scanners. The spatial resolution of these systems ranges between 3–4.5 mm full-width at half-maximum (FWHM). As noted in the table, the sensitivities range from 5 kcps/MBq for the 16-cm AFOV Philips Vereos to almost 21 kcps/MBq for the 25-cm AFOV GE Discovery MI.

While the image quality of a standard AFOV PET scanner is generally excellent, there are a number of imaging scenarios where a longer AFOV would be advantageous[22,23]. A standard AFOV scanner only detects 0.5–2% of the emitted coincident events from a 70-cm long line source (as in the standardized NEMA sensitivity measurement[21]) due to its short axial coverage. This relatively low sensitivity makes it difficult to image radioisotopes with a low positron fraction (e.g., ^{89}Zr, ^{90}Y) or radiotracers with slower biological clearance (e.g., FDG, where delayed imaging beyond the current 1 hour post-injection would enable imaging lesions with higher contrast). In addition, the 1–3 min/bed position still results in relatively long total scan durations, with the possibility of patient motion and discomfort; imaging with higher sensitivity enables the total scan time to be reduced significantly. It also opens up the possibility of improved imaging in obese patients as well as imaging with reduced injected activity in situations where radiation dose may be considered limiting (e.g., pediatric patients, serial studies to assess treatment response).

2. History of long AFOV scanners

2.1 Techniques to increase sensitivity

One method to increase the sensitivity is to increase the solid angle of detection of the annihilation photons by reducing the diameter of the detector rings; moving the detectors closer to the object allows for more coincidences to be detected[24]. This is one rationale for designing PET scanners that are dedicated to specific organ imaging (e.g., brain PET or breast PET systems). However, this happens at the expense of increased detection of unwanted random and scattered coincidences, as well as worse spatial resolution due to parallax errors off-center. For whole-body imaging, there is a limit on how much the ring diameter can be reduced, as well: in the case of the thorax and abdomen there is little ability to reduce the bore diameter without making it impossible to scan more obese patients.

Another technique to increase sensitivity is to use longer crystals. The mean stopping distance for 511-keV photons in LSO/LYSO is ~11 mm, while the length of crystals used in most systems is 18–20 mm. There are diminishing returns in the gain in efficiency as the crystal length is increased[25], while the detector material cost still increases linearly. Only incremental gains in sensitivity can be achieved by lengthening the crystals beyond the ~20 mm typically used in today's scanners. Note that the converse is not the case: using shorter crystals to decrease the cost of a system leads to a measurable loss of sensitivity[25].

Using a different crystal with a higher stopping power than LSO/LYSO is another way to increase the sensitivity of a scanner. However, 20 mm of bismuth germanate (BGO), one of the most dense scintillators discovered, has only ~1.07 times the coincidence detection efficiency as the same thickness of LSO/LYSO. Once more, these gains are fairly incremental. In addition, with every crystal there are potential trade-offs in energy and timing resolutions, ease of growing, cost, crystal handling, etc.

Improving the timing resolution of a scintillator will also lead to increased effective sensitivity and reduced image noise for the same number of detected events because TOF reconstruction can localize the events along the LOR rather than spreading them out uniformly. This has been the rationale for PET scanner manufacturers to continue to improve the TOF resolution of their systems from 600 ps for the Philips Gemini TF, the first commercial TOF PET scanner, to 215 ps for the latest Siemens Vision. It is possible further significant gains can be made in this area; however, new detector technology and/or alternative signal generation mechanisms (e.g., prompt luminescence from Cerenkov radiation) are likely required[26].

The most obvious and effective means of significantly increasing the sensitivity of a PET scanner, however, is to make it longer by adding more detectors along the axial direction. By accepting events along more oblique LORs (larger axial acceptance angle) and covering more of the body with detectors, very significant increases in detection sensitivity are possible[27]. This is the driving force behind the recent development of long AFOV PET scanners.

2.2 Early long AFOV designs

There have been a number of proposed designs for long AFOV scanners to increase the system sensitivity. In the early 2000s, a number of scanners with extended AFOV were proposed using different detector technologies. Hamamatsu developed a 68.5-cm AFOV system based on BGO detectors[28] with coarse septa between block detector rings to reduce detected scatter, since the energy resolution of BGO is poor (36%) although these septa also reduced the sensitivity advantage of the longer AFOV. Conti, et al., developed a research PET system with a 53-cm AFOV based on five large panel LSO detectors on a rotating gantry[29]. This system had large deadtime losses that led to noisy images and lacked TOF capability. Zhang and Wong proposed a 1-m long scanner composed of BGO crystals in a quadrant-sharing arrangement[30]. Since BGO has a long decay time, it was proposed as a nonTOF system although the estimated sensitivity was higher than that of a standard AFOV TOF PET scanner. Crespo proposed a 2.4-m long system with resistive plate chamber (RPC) detectors as an inexpensive alternative to scintillators[31]. These detectors have a TOF resolution of 300 ps and excellent spatial discrimination but low stopping power and poor energy resolution that reduce the intrinsic sensitivity of the detectors. In the end, however, each of these designs involved compromises in performance, required the long axial coverage to make up for performance losses, or were not cost-effective, and they did not become clinical systems.

2.3 Simulation studies

The interest in long AFOV systems, though, sparked a number of simulation studies to examine the impact on performance of possible design choices. Eriksson, et al., looked at the impact of both faster scintillators and large AFOV (up to 2.2 m) on system performance and found advantages for sub-minute whole-body scan times and dynamic imaging[32]. Poon, et al., also considered the optimal scanner geometry (AFOV, crystal thickness) for a range of crystal volumes with a coincidence timing window that was allowed to vary with ring difference[27]. Surti, et al., used simulations to study the optimal use of a given amount of

crystal material and found the best lesion detectability was for scanners with long AFOV and short crystals[25]. Later work considering optimal detector designs for a 72-cm long scanner for both lesion detection and quantification showed that improving the TOF resolution led to significant gains in performance, while using smaller crystals or depth-of-interaction (DOI) information to reduce parallax errors provided only small gains in detectability[33]. Schmall, et al., demonstrated that even for a 2-m long scanner, the axial resolution degradation was small compared with radial parallax errors and could be mitigated with two-layer DOI information[34], although DOI adds complexity to the detector design.

3. Detector technology considerations for long AFOV scanners

This section focuses on choices and trade-offs in selecting detector technology for long AFOV scanners, where care must be taken to ensure the performance is sufficient to allow the predicted benefits of these systems to be realized in clinical studies, while accounting for the challenges in developing such large, complex systems that relate to cost, reliability, and the need to handle very high total event rates.

3.1 Crystal technology

As with conventional PET scanners, lutetium-based scintillators such as LSO or LYSO are currently the material of choice for most long AFOV scanners. These are currently the only materials that can deliver sufficient stopping power and are also bright and fast enough to provide timing resolution of a few hundred picoseconds, energy resolutions of around 10–14%, and relatively low deadtime. The disadvantage, which is not an insignificant one, is that these materials are quite expensive, and with the large quantities required for long AFOV scanners (0.5 ton or even more), these systems will be expensive. Therefore, alternatives are being studied. One interesting possibility is the use of BGO, which emits both scintillation light and, as only recently exploited, prompt Cerenkov radiation emitted by the energetic electrons produced upon absorption of the annihilation photon. The Cerenkov photons can be used to achieve much better timing resolution than was thought possible with this material[35,36]. While attractive due to its cost (~1/3 that of LSO or LYSO), a significant challenge remains how to reliably detect and trigger on the very faint Cerenkov signals with cost-effective electronics.

3.2 Photodetector technology and detector designs

SiPMs have become the photodetector of choice for modern PET scanners, and their detection sensitivity for scintillation light, reliability, low power consumption, low applied voltage, compact form factor, and relatively low cost are all advantages that are further amplified in the setting of long AFOV PET scanners that use very large numbers of these devices.

There are a couple of choices in how SiPMs are used in conjunction with scintillation crystals. The first is known as 1:1 coupling, in which each scintillator crystal element has its own SiPM readout (Figure 1A). This leads to the best performance in terms of light collection, which in turn leads to good timing and energy resolution. Also, the crystal of

interaction is simply identified by knowing which SiPM produced the signal. The one downside of this approach is that a PET scanner needs a large number of SiPMs, each with its own channel of readout electronics. Conventional scanners have on the order of 50,000 crystal elements. This challenge is exacerbated in long AFOV scanners where the number of crystal elements and therefore SiPMs required can exceed 500,000.

An alternative is a light sharing approach in which an array of scintillation crystals is read out by a smaller number of SiPMs (Figure 1B). Light produced in each scintillation crystal is allowed to spread across multiple SiPMs (typically by use of a light guide) and the relative signals in neighboring SiPMS are then used to compute the center of the light distribution and thus determine the crystal of interaction. However, by spreading the light among multiple SiPMs, with small gaps between them, the light collection is not as good, and the signals in each SiPM are smaller, compared to 1:1 coupling. Also, the effective area of the detector that is "busy" while processing an event is larger with this approach, potentially leading to increased overlap of events and deadtime at high counting rates. This leads to some degradation in performance, with the benefit, however, of a much-reduced number of SiPMs and channels of electronics. Both these approaches have been successfully implemented in long AFOV PET scanners as described later.

3.3 Alternate detector technologies

There are a range of alternate detector technologies being pursued for long AFOV PET scanners, often aimed primarily at reducing cost rather than improving performance relative to existing LYSO/SiPM-based systems. As already mentioned, BGO is being explored as an alternative scintillator material given its lower cost and higher density that allows one to use somewhat less material compared to LSO or LYSO for the same detection efficiency. The challenge is to get sufficient timing performance and count rate capability to be competitive with traditional LYSO-based designs. Another approach proposes the use of a "monolithic" block of scintillator material, read out by an array of SiPMs, rather than an array of individual scintillator elements[37] (Figure 1C). This geometry favors collection of the scintillation light and can therefore lead to very good energy and timing resolution. However, positioning of each event is more complicated, especially towards the edges of the block where the light distribution is constrained by the edge of the crystal. Recent results from the University of Ghent with a 16-mm thick monolithic detector have demonstrated that excellent performance can be achieved with these detectors when appropriate care is taken[38].

4. General scanner design considerations

4.1 Choice of axial FOV

One of the biggest debates as long AFOV PET scanners are being developed is regarding the optimal length of the scanner. There is no "right' answer, since the question must be framed with respect to the intended application, and currently no comprehensive studies exist that evaluate the cost to benefit ratio for a given clinical task as a function of axial scanner length. Therefore, this debate will likely continue unabated for some time to come.

Some of the considerations can be clearly stated. A significant majority of clinical PET studies are for oncology and involve imaging from “eye to thighs” in order to see distant metastases. Based on anthropometry studies[39,40], this distance averages about 83 cm across the adult population. In the particular case of melanoma, often the entire body from head-to-toe needs to be scanned. The average height (women and men) for the US population is around 170 cm, with the 95th percentile being at 189 cm for men.

For research studies, and possible future clinical applications of PET, which may involve imaging other systemic diseases (e.g., infection) or multi-organ/tissue effects (e.g., inflammation), it likely will be important to image at least all the major organs from brain to pelvis (95th percentile length is ~97 cm), and in some cases (e.g., rheumatoid arthritis) one again may need to image the entire body to characterize disease in all the joints. Based on these considerations, the minimum AFOV for single bed position imaging is around 85–90 cm for “eyes-to-thighs’ coverage across the majority of the population, around 1 m for coverage of all the vital organs, and close to 2 m for coverage of the entire human body.

Next one has to factor in the sensitivity profile of the PET scanner, which to first order is roughly triangular in shape without attenuation, as shown in Figure 2. However, one also must account for the fact that the most oblique lines of response traverse a very large amount of tissue and due to attenuation and scatter contribute little useful information; with attenuation the sensitivity profile becomes flatter[33,34]. Therefore, a cut in the axial acceptance angle on the order of about 50–60° is often applied to remove events at these steep angles that contribute little useful information. If one wants to take advantage of high and relatively uniform sensitivity across a given region, one therefore sees that the scanner actually needs to be somewhat longer than the desired body coverage; otherwise tissues near the ends of the field of view will be imaged with low detection sensitivity.

The anthropometry data and the scanner sensitivity profiles, therefore, suggest that to achieve high sensitivity coverage of all the major organs of the body (brain to prostate/uterus), the scanner would need to have a length of at least ~140 cm to image this field in a single bed position (Figure 2). Of course, one may choose a shorter length and multi-bed position imaging for cost considerations; however, then the ability to acquire high quality dynamic data across all the major organs is sacrificed. There remains a range of opinions on the “optimal” AFOV that largely depend on how one balances the value of the increased sensitivity and body coverage as the scanner gets longer with the trade-off of increasing cost.

One proposed technique to increase the AFOV while controlling costs is to design the scanner with incomplete detector coverage (i.e., gaps between detectors in various configurations). A long AFOV TOF-PET scanner with this design would take advantage of the ability of TOF reconstruction to handle missing information better than non-TOF reconstruction[41,42]. A number of groups have studied various designs involving incomplete detector coverage[38,43–49], although few such systems have been built. The tradeoff is a significant loss of sensitivity (often by a factor >2) with axial variations in sensitivity that translate to small differences in noise across the AFOV. The development of these systems has largely been through simulations or extrapolations from standard AFOV systems, although we can expect further developments in this area in the future. As described in Sec.

5.2, although not built with missing detectors, the PennPET Explorer scanner currently operates with 7.6-cm such gaps between rings, thereby demonstrating the feasibility of these designs for total-body PET imaging.

4.2 Multimodal long AFOV scanners

Long axial FOV scanners are no different in needing additional information for attenuation and scatter correction that typically will come from an integrated CT scanner. Large AFOV coverage will benefit from development of low-dose helical CT acquisitions[50] utilizing advanced low-noise x-ray detectors, automatic tube current modulation, optimized beam filtering, and iterative reconstruction, as well as denoising methods using deep learning[51]. This will be important for low-activity PET applications, where the CT component then becomes the dominant source of radiation dose to the subject.

Another option is to integrate large AFOV PET scanners with MRI systems. While scientifically appealing due to the rich variety of image contrast that could then be assessed by MRI, as well as the elimination of the radiation dose from CT, current state-of-the-art MR systems do not have sufficient axial coverage for single bed position imaging of all the major organs. Developing MRI systems with a homogeneous magnetic field and the necessary gradients over a meter or more would likely be quite challenging and expensive. Nonetheless, it is an area that should be further studied.

4.3 Technical design considerations

There are several technical and engineering considerations in large AFOV scanners. First, the number of components is 5–10-fold higher than in a conventional PET scanner, and therefore components need to be extremely robust and reliable in order to maintain scanner operations in a busy clinical environment. In addition to careful sourcing and selection of components, tight power regulation and temperature control also are important factors in ensuring scanner stability. Early experience with the two long AFOV scanner designs currently in use have demonstrated good reliability of the many detectors and components.

The patient bed also must be carefully designed, especially if a CT scanner is present as part of the system, where deflection of the bed as it moves into the PET field of view, under varying loads, must be avoided or known in order to ensure that the CT and PET are properly spatially registered.

One major difference from conventional PET scanners is the greatly increased length of the “tunnel” into which the patient is placed. Careful design of the tunnel (for example lighting, air flow, etc.) is desirable to reduce the chance of claustrophobia. Cameras and microphones are helpful for communication with the patient, and for research studies that may involve on-bed injection and/or blood sampling, access to injection and sampling sites, as well as the length and deadspace in long tubing, require thought and appropriate methods and protocols.

One design simplification in long AFOV scanners is the fact that end shields to reduce scatter from outside the scanner are not necessary if the entire body, or most of the body, is within the field of view of the scanner. However, shielding between the CT component and

the PET system may still be necessary to avoid the high x-ray flux from CT causing any long-lived luminescence in the PET detectors.

Lastly, the wide range of path lengths through the body dictate the need for variable timing windows. If one assumes a body diameter of 40 cm, the path length that photon pairs travel through the body can range from roughly 40 cm to 70 cm at an axial angle of 60°, requiring that the coincidence timing window is varied according to the path length for best rejection of random coincidences (Figure 3).

5. Design specifics of long AFOV scanners

There are currently two operational long AFOV PET scanners: the uEXPLORER co-developed by the University of California, Davis (UC Davis) and United Imaging Healthcare and the PennPET Explorer designed and built at the University of Pennsylvania (UPenn). Both of these efforts were supported through the EXPLORER consortium, which was set up in 2011 to develop long AFOV PET scanners and funded by the National Institutes of Health in 2015. In designing both of these systems, the goal was to maintain the performance of standard AFOV clinical PET scanners (e.g., spatial, timing, and energy resolutions) while extending the AFOV in order to explore the potential benefits and applications of these long systems. The optimal AFOV and scanner design is as yet undetermined. Having two systems of different designs allows us to probe the impact of design characteristics on clinical performance. Table 2 summarizes the performance characteristics of the two systems.

5.1 uEXPLORER

The uEXPLORER PET/CT scanner (Figure 4) was designed to be the first PET scanner capable of imaging the entire human body at once with an emphasis on extremely high detection sensitivity and spatial resolution[52]. Each detector module consists of a 6 × 7 array of 2.76 × 2.76 × 18.1 mm LYSO crystals, read out by four 6-mm square SiPMs. These modules are assembled into rectangular panels, which are then arranged in rings to form a scanner with a ring diameter of 78.6 cm and an axial extent of 194 cm. There are a total of 13,440 modules (564,480 crystals) in the entire system. The axial acceptance angle is restricted to 57° and the timing windows are variable from 4.5 to 6.9 ns depending on the path length across the scanner. The standard energy window is 430–645 keV. An 80detector row, 160-slice CT scanner is integrated on the front of the system.

The sensitivity for a 170-cm long line source (which corresponds to the average length of the human body) is 147 kcps/MBq at a radius of 0 cm. For comparison, the sensitivity for a 170-cm long line source on a conventional length scanner would be 2.4–8.6 kcps/MBq, a factor of 17–60 lower than the uEXPLORER. The spatial resolution, measured using the standardized NEMA test[21] with simple filtered backprojection reconstruction, is ~ 3 mm, and can be improved using more sophisticated iterative reconstruction methods which are routinely used for clinical scans. The time of flight resolution, again using NEMA methods, is 509 ps. The system is 510(k) cleared and has been in use for clinical and research studies since August, 2018[53].

5.2 PennPET Explorer

The PennPET Explorer scanner (Figure 5) was designed as a scalable system with an emphasis on high sensitivity with excellent TOF resolution[54]. The PennPET Explorer is based on the detector tile of 64 LYSO crystals currently used in the Philips Vereos PET/CT scanner. Each 8 × 8 array of 3.86 × 3.86 × 19 mm^3 crystals is coupled to a digital SiPM developed by Philips Digital Photon Counting. There is 1:1 crystal-sensor coupling. The entire gantry and electronics are water-cooled to allow for superior timing resolution. A detector ring is 76.4 cm in diameter and 22.9 cm axially, comprising 18 modules of 28 detector tiles in a 4 × 7 array. The rings are designed to be stacked axially with a 1-cm physical gap between rings. The prototype 3-ring configuration, for which performance results have been described, was limited to reading out only 5 (of the total 7) rows of tiles in each ring, for a total AFOV of 64 cm and 7.6-cm gaps (corresponding to the 2 inactive rows) between each ring. The transverse FOV is set in software to 57.6 cm. The axial acceptance angle is not currently restricted; the 3-ring prototype had a maximum acceptance angle of ±40°. The scanner is in the process of being extended to 6 rings for a final AFOV of 140 cm, where the maximum acceptance angle will be ±62°.

The sensitivity of the 3-ring prototype PennPET Explorer for a 170-cm long line source is 23 kcps/MBq at a radius of 0 cm; for a 5-ring configuration with an AFOV of 112 cm, the sensitivity has increased to 35 kcps/MBq, a factor of ~4–15 times higher than conventional length scanners. The data readout gaps reduce the total sensitivity by a factor of 2 from what would be achieved with all crystals active. The scatter fraction is 32% and is stable over activity concentrations up to 38 kBq/mL, and the trues rate is linear over this range, as well. When cooled to 5° C, the TOF resolution is 256 ps. The spatial resolution is 4.0 mm using filtered backprojection reconstruction. The scanner has been in use for research studies since August, 2018[55].

6. Measurement of performance of long AFOV systems

The goal of performance standards for PET is to characterize both intrinsic and overall performance in a reproducible, straightforward way so that systems can be meaningfully compared and performance can be validated against specifications (e.g., NEMA NU 2 PET Standards[21]). While measurements of intrinsic performance (i.e., spatial resolution, sensitivity, count rate performance, scatter fraction) are done using activity distributions or reconstruction algorithms that are not clinically relevant, nonetheless the results are indicative of scanner behavior; for example, a system with low intrinsic sensitivity will have higher image noise than one with high sensitivity, although the sensitivity value will not predict the number of acquired events in a clinical scan. This means, however, that the measurements should similarly indicate relative performance for both standard and long AFOV systems, while providing relevant performance metrics that capture system-wide performance.

The NEMA PET scanner performance standards were originally developed in the early 1990s when it was inconceivable that a scanner would ever be longer than 65 cm, and the tests were only designed to accommodate these shorter systems[56,57]. The spatial resolution is measured with point sources at radial positions of 1 and 10 cm, axially positioned at the

center of the AFOV and 3/8 of the AFOV from the center. The sensitivity is measured with a 70-cm long line source in a set of 5 aluminum sleeves to measure both total sensitivity and the axial sensitivity profile along the system. Count rate performance and scatter fraction are measured using the same 70-cm long line source but positioned off-center inside a 20-cm diameter polyethylene cylinder. Finally, the image quality phantom is the 18-cm long International Electrotechnical Commission (IEC) torso phantom positioned with the spheres (diameters: 10 – 37 mm) at the center of the AFOV with the count rate performance phantom abutted at one end to emulate activity from outside the AFOV of the scanner.

As the scanner AFOV increases, the question arises of how to measure and report the performance of these systems. One could imagine simply extending the NEMA phantoms to 2 m long, for example, to cover the largest conceivable PET scanner to date. However, in addition to being extremely cumbersome to fill and handle, it is not apparent that these phantoms will provide performance information that is at all relevant to clinical imaging. A typical human is not well-represented by a 20-cm cylinder that is 2 m long; most of the organs of interest are contained within 100–120 cm, depending on the study, and the average height of a human is around 170 cm. Measuring the sensitivity with a source longer than that inflates the number of events that would be present in human imaging, and both UC Davis and UPenn have chosen to measure and report sensitivity for a 170-cm long line source. On the other hand, a 70-cm long line source does not reflect the activity distribution in human imaging, either. As seen in Table 2, the sensitivity values for a 170-cm line source are not easily compared to the current NEMA measure with a 70-cm line source. In addition, while a uniform cylinder that extends through the full AFOV is helpful to demonstrate that all corrections work properly throughout the entire scanner, it is cumbersome to handle and difficult to fill uniformly. As seen in Figure 5b, a 10-cm diameter cylinder was used for this purpose on the PennPET Explorer, since it is lighter and more practical than the traditional 20-cm cylinder, although a special apparatus is needed to ensure uniform mixing.

There are also unique performance characteristics of long AFOV systems that warrant measurement. These include axial blurring resulting from the very large axial acceptance angle that can lead to variation in the axial spatial resolution across the AFOV (although simulations[34] and early results[52,54] indicate that the degradation is far smaller than that due to radial parallax errors); increase in multiple scatter events and the impact on the accuracy of the scatter correction especially at the center of the AFOV; increase in random coincidences and multiple coincidences (>2 photons arriving within the coincidence timing window) and their impact on the maximum activity that should be injected; and sensitivity measured in both air and an attenuating medium because oblique LORs that contribute to the overall increase in total sensitivity when measured in air are more likely to be attenuated by the patient due to their longer pathlengths through the body. In measuring the performance of their long AFOV systems, both UPenn and UC Davis modified and enhanced the NEMA standard measurements to address some of these issues, but further work is needed to reach a consensus on performance measurements that characterize all PET scanners reproducibly and meaningfully.

7. Data and computational challenges with long AFOV systems

One major consideration related to the use and associated computational infrastructure for long AFOV PET systems derives from the large amounts of data these systems produce, and the necessity for robust and reliable procedures for reconstructing, storing, and analyzing this data.

7.1 Event rates and data storage

The number of lines of response measured by the uEXPLORER scanner, already accounting for the restricted axial acceptance angle, is 92 billion. As the number of possible LORs greatly exceeds the number of events that will be acquired, it is therefore most efficient to store the raw data in list mode format rather than binning into projections or sinograms. There also is a trade-off between how much information is retained for each event (for example is the energy information retained after the energy window has been satisfied) and the size of the list mode dataset.

For a typical clinical scenario (370-MBq injected dose of FDG, 60 min uptake time), the uEXPLORER registers on the order of 10 million prompt coincidence events per second. A ten min scan will produce roughly 12 billion prompt events and produce a list mode file on the order of 200 GB in size. For a 60-min dynamic acquisition starting from the time of injection, the dataset size can easily exceed 1 TB. On the 5-ring PennPET Explorer, where singles data are acquired and processed concurrently in software to form coincidences, an FDG scan with similar injected dose produces about 190 GB of singles events for a final coincidence list file that is 70 Gb. It is not certain that the singles list data will be routinely archived, although access to singles information may prove advantageous for data corrections (e.g., scatter and randoms). Nevertheless, methods to efficiently move, and potentially archive, these large datasets must be considered.

7.2 Image reconstruction

All modern PET scanners use sophisticated iterative reconstruction methods based on ordered subsets expectation maximization (OSEM) algorithms[58] that permit detailed modeling of the scanner geometry and the statistical nature of the underlying data. However, there is always a trade-off between the complexity of the modeling and reconstruction time, and nowhere is this more challenging than for long AFOV scanners, which produce high quality data that would benefit from the most sophisticated modeling approaches, yet at the same time produce large datasets that will be reconstructed into large image volumes, producing severe challenges in terms of computation and memory requirements. For routine clinical purposes, one requires a reconstruction time on the order of a few minutes per scan, and this may require the use of simplifying assumptions within the reconstruction algorithm that may not fully optimize spatial resolution or contrast-tonoise ratio. For research studies, longer reconstruction times may be acceptable; however, these studies may also involve dynamic imaging and produce larger datasets, and reconstruction times (including the need to compute scatter correction files for each frame of a dynamic dataset) can easily run into many hours on a high-end computer cluster.

7.3 Image storage and analysis

Scans from long AFOV PET scanners are often reconstructed into somewhat smaller voxel sizes than on regular scanners, because the higher signal-to-noise ratio supports high resolution reconstructions. For example, on the uEXPLORER scanner, a typical image matrix size for clinical scans is 256 × 256 × 828 (2.34 mm isotropic voxels); PennPET Explorer images are 288 × 288 × 560 (2 mm isotropic voxels). While this is not particularly onerous, the image dataset sizes rapidly expand for dynamic studies, exacerbated for long AFOV scanners that can not only support higher spatial resolution, but also higher temporal resolution (more frames). For example, a 66-frame dynamic scan on the uEXPLORER results in an image dataset size of about 7.2 GB that can pose challenges for much of the software developed for analyzing dynamic PET data due to memory limitations.

8. Further improvements in PET systems with a focus on long AFOV designs

While these first long AFOV systems have verified the large sensitivity gains that were predicted and are now being deployed in a range of clinical and research applications to provide data on the benefits of this sensitivity gains, future improvements are clearly possible. The performance capabilities of the uEXPLORER and PennPET Explorer scanners, both based on existing technology, together with a better understanding of the benefits of long AFOV systems for clinical studies and research investigations will help to form the basis for next generation systems.

Now that the geometric coverage is close to a maximum; further significant gains in effective sensitivity through instrumentation are only going to come from major improvements in timing resolution. Future approaches or technologies that could push the system timing resolution well below 100 ps would be worthy of pursuit, noting that a timing resolution as good as 20 ps would localize the site of annihilation with sufficient accuracy to eliminate the need for any image reconstruction[26].

Modest performance improvements would also come from depth-encoding detectors[38] that could reduce or eliminate parallax errors and ensure the spatial resolution is uniform across the field of view, as well as new detector materials with better stopping power, especially higher photoelectric cross-sections, which would somewhat improve detector efficiency and spatial resolution.

Electronics, photodetectors, and signal processing are other areas where improvements are possible. For example, the tasks of estimating event position, timing, and energy from detector pulses may be amenable to deep-learning networks, and fast photodetectors possibly with integrated on-chip circuits for optimized timing performance will play an important role in achieving better time-of-flight information. Advanced image reconstruction algorithms that accurately model the physics and statistics of the event formation process, and/or the use of deep-learning approaches during or post-image reconstruction[59], promise further improvements in performance for a given hardware configuration.

Lastly, and justifiably, there will continue to be a focus on detector technologies that can achieve a large AFOV but at a significantly reduced cost. In truth, many of these approaches involve significant sacrifices in sensitivity or other performance parameters, but they may still lead to systems that are adequate for specific and important clinical tasks or research investigations. Approaches being investigated include different detector materials such as plastic scintillators[60] or resistive plate chambers[31]. As discussed earlier, sparse detector configurations are also being pursued, where holes or gaps are introduced to reduce cost[46,47,49] while still providing sufficient data sampling to reconstruct images of the body. One challenge with this approach is that while the cost is roughly linear with detector area, the coincidence efficiency goes as approximately the square of the detector area. Thus, a scanner in which 1/4 of the detectors are removed reduces the cost by about 25%, but the coincidence sensitivity will be roughly $(0.75)^2$=0.56 of its original value, meaning that ~44% of the signal will have been lost. This trade-off between cost and sensitivity rapidly becomes unattractive as more detector material is removed.

9. Conclusions

Long AFOV PET scanners have recently been built that take advantage of the latest innovations in PET technology. These systems provide extended axial coverage (≥70 cm) that allows coverage of most major organs up to the total body (depending on AFOV) in a single bed position with ultra-high sensitivity without compromising performance in other areas. The uEXPLORER developed by UC Davis and United Imaging Healthcare and the PennPET Explorer developed at UPenn have demonstrated the performance possible with long AFOV systems while also highlighting the challenges associated with these systems, including design and cost considerations as well as the need for a robust computational infrastructure. As we gain clinical and research experience with long AFOV scanners, it is envisioned that long AFOV scanner technology will develop along different paths. Improvements in scanner performance (e.g., TOF, energy, and spatial resolutions) will be driven by advances in detection and signal processing technology while systems will also be developed that are more cost-effective using lower cost detectors or sparse detector coverage to allow for more widespread availability. Long AFOV scanner development is still in its infancy, and its future will depend largely on the observed benefits and unique applications of this very exciting technology.

10. References

1. Karp JS, Muehllehner G, Mankoff DA, Ordonez CE, Ollinger JM, Daube-Witherspoon ME, Haigh ME, Beerbohm DJ. Continuous-slice PENN-PET: A positron tomograph with volume imaging capability. J Nucl Med 1990;31:617–627. [PubMed: 2341898]
2. Cherry SR, Dahlbom M, Hoffman EJ. PET using a conventional multislice tomograph without septa. J Comput Assist Tomogr 1991;15:655–668. [PubMed: 2061484]
3. Ter-Pogossian MM, Mullani NA, Ficke DC, Markham J, Snyder DL. Photon time-of-flight-assisted positron emission tomography. J Comput Assist Tomogr 1981;5:227–239. [PubMed: 6971303]
4. Snyder DL, Thomas LJ, Ter-Pogossian MM. A mathematical model for positron emission tomography systems having time-of-flight measurements. IEEE Trans Nucl Sci 1981;28:3575–3583.

5. Politte DG, Snyder DL. Results of a comparative study of a reconstruction procedure for producing improved estimates of radioactivity distributions in time-of-flight emission tomography. IEEE Trans Nucl Sci 1984;NS-31:614–619.
6. Allemand R, Gresset C, Vacher J. Potential advantages of a cesium fluoride scintillator for a time-of-flight positron camera. J Nucl Med 1980;21:153–155. [PubMed: 6965404]
7. Mullani NA, Ficke C, Ter-Pogossian MM. Cesium fluoride: A new detector for positron emission tomography. IEEE Trans Nucl Sci 1980;NS-27:572–575.
8. Wong WH, Mullani NA, Wardworth G, Hartz RK, Bristow D. Characteristics of small barium fluoride (BaF_2) scintillator for high intrinsic resolution time-of-flight positron emission tomography. IEEE Trans Nucl Sci 1984;NS-31:381–386.
9. Melcher C, Schweitzer JS. Cerium-doped lutetium oxyorthosilicate: a fast, efficient new scintillator. IEEE Trans Nucl Sci 1992;39:1161–1166.
10. Surti S, Kuhn A, Werner ME, Perkins AE, Kolthammer J, Karp JS. Performance of Philips Gemini TF PET/CT scanner with special consideration for its time-of-flight imaging capabilities. J Nucl Med 2007;48:471–480. [PubMed: 17332626]
11. Jakoby BW, Bercier Y, Conti M, Casey M, Bendriem B, Townsend DW. Physical and clinical performance of the mCT time-of-flight PET/CT scanner. Phys Med Biol 2011; 56:2375–2389. [PubMed: 21427485]
12. Zhang J, Maniawski P, Knopp MV. Performance evaluation of the next generation solid-state digital photon counting PET/CT system. EJNMMI Res 2018;8:97. [PubMed: 30402779]
13. van Sluis J, de Jong J, Schaar J, Noordzij W, van Snick P, Dierckx R, et al. Performance characteristics of the digital Biograph Vision PET/CT system. J Nucl Med 2019;60:1031–1036. [PubMed: 30630944]
14. Pan T, Einstein SA, Kappadath SC, Grogg KS, Lois Gomez C, Alessio A, et al. Performance evaluation of the 5-Ring GE Discovery MI PET/CT system using the National Electrical Manufacturers Association NU 2–2012 Standard. Med Phys 2019;46:3025–3033. [PubMed: 31069816]
15. Degenhardt C, et al. The digital silicon photomultiplier: A novel sensor for the detection of scintillation light. In: Yu B, editor. Conference Record of the 2009 IEEE Nuclear Science Symposium and Medical Imaging Conference Piscataway, NJ: IEEE; 2009 p. 2383–2386.
16. Karakatsanis NA, Lodge MA, Tahari AK, Zhou Y, Wahl RL, Rahmim. Dynamic whole-body PET parametric imaging: I. Concept, acquisition protocol optimization and clinical application. Phys Med Biol 2013;58:7391. [PubMed: 24080962]
17. Osborne DR, Acuff S. Whole-body dynamic imaging with continuous bed motion PET/CT. Nucl Med Comm 2016;37:428–431.
18. Hsu DFC, Ilan E, Peterson WT, Uribe J, Lubberink M, Levin CS. Studies of a next-generation silicon-photomultiplier-based time-of-flight PET/CT system. J Nucl Med 2017;58:1511–1518. [PubMed: 28450566]
19. Chen S, Hu P, Gu Y, Yu H, Shi H. Performance characteristics of the digital uMI550 PET/CT system according to the NEMA NU2–2018 standard. EJNMMI Phys 2020;7:43. [PubMed: 32588139]
20. Li X, Qi W, Miyahara M, Kolthammer J. Performance characterization of an SiPM-based time-of-flight Canon PET/CT scanner. J Nucl Med 2020;61S:1505 (abstract).
21. NEMA Standards Publication NU 2–2018, Performance Measurements of Positron Emission Tomographs (PET). Rosslyn, VA: National Electrical Manufacturers Association, 2018.
22. Cherry SR, Badawi RD, Karp JS, Moses WW, Price P, Jones T. Total-body imaging: Transforming the role of positron emission tomography. Sci Transl Med 2017;9eaaf6169.
23. Cherry SR, Jones T, Karp JS, Qi J, Moses WW, Badawi RD. Total-body PET: Maximizing sensitivity to create new opportunities for clinical research and patient care. J Nucl Med 2018;59:3–12. [PubMed: 28935835]
24. Nakanishi K, Hirano Y, Yamamoto S. Comparison of noise equivalent count rates (NECRs) for the PET systems with different ring diameter and electronics. IEEE Trans Radiat Plasma Med Sci 2019;3:371–376.

25. Surti S, Werner ME, Karp JS. Study of PET scanner designs using clinical metrics to optimize the scanner axial FOV and crystal thickness. Phys Med Biol 2013;58:3995–4012. [PubMed: 23685783]
26. Lecoq P, Morel C, Prior J, et al. Roadmap towards the 10 ps time-of-flight PET challenge. Phys Med Biol (in press). 10.1088/1361-6560/ab9500.
27. Poon JK, Dahlbom ML, Moses WW, et al. Optimal whole-body PET scanner configurations for different volumes of LSO scintillator: a simulation study. Phys Med Biol 2012;57:4077–4094. [PubMed: 22678106]
28. Watanabe M, Shimizu K, Omura T, Sato N, Takahashi M, Kosugi T, Ote K, Katabe A, Yamada R, Yamashita T, Tanaka E. A high-throughput whole-body PET scanner using flat panel PS-PMTs. IEEE Trans Nucl Sci 2004;53:1136–1142.
29. Conti M, Bendriem B, Casey M, Eriksson L, Jakoby B, Jones W, Jones J, Michel C, Nahmias C, Panin V, et al. Performance of a high sensitivity PET scanner based on LSO panel detectors. IEEE Trans Nucl Sci 2006;53:1136–1142.
30. Zhang Y, Wong WH. Design study of a practical-entire-torso PET (PET-PET) with low-cost detector design. In: Conference Record of the 2016 IEEE Nuclear Science Symposium and Medical Imaging Conference Piscataway, NJ: IEEE; 2016.
31. Crespo P, Reis J, Couceiro M, Blanco A, Ferreira NC, Ferreira Marques R, Martins P, Fonte P. Whole-body single-bed time-of-flight RPC-PET: Simulation of axial and planar sensitivities with NEMA and anthropomorphic phantoms. IEEE Trans Nucl Sci 2012;59:520–529.
32. Eriksson L, Conti M, Melcher CL, Townsend DW, Eriksson M, Rothfuss H, Casey ME, Bendriem B. Towards sub-minute PET examination times. IEEE Trans Nucl Sci 2011;58:76–81.
33. Surti S, Karp JS. Impact of detector design on imaging performance of a long axial field-of-view, whole-body PET scanner. Phys Med Biol 2015;60:5343–5358. [PubMed: 26108352]
34. Schmall JP, Karp JS, Werner M, Surti S. Parallax error in long-axial field-of-view PET scanners – a simulation study. Phys Med Biol 2016;61:5443–5455. [PubMed: 27367971]
35. Kwon SI, Gola A, Ferri A, Piemonte C, Cherry SR. Bismuth germanate coupled to near ultraviolet silicon photomultipliers for time-of-flight PET. Phys Med Biol 2016;61:L38–L47. [PubMed: 27589153]
36. Brunner SE, Schaart DR. BGO as a hybrid scintillator / Cherenkov radiator for cost-effective time-of-flight PET. Phys Med Biol 2017;62:4421–4439. [PubMed: 28358722]
37. Borghi G, Tabacchini V, Bakker R, Schaart DR. Sub-3mm, near-200 ps TOF/DOI-PET imaging with monolithic scintillator in a 70 cm diameter tomographic setup. Phys Med Biol 2018;63:155006. [PubMed: 29995639]
38. Vandenberghe S, Mikhalyova E, Brans B, Defrise M, Lahoutte T, Muylle K, et al. PET 20.0: A cost efficient, 2.00 mm resolution total body monolithic PET with very high sensitivity and an adaptive axial FOV up to 2.00 m. Presented at EANM, 2019.
39. McDowell MA, Fryar CD, Ogden CL, Flegal KM. Anthropometric Reference Data for Children and Adults: United States, 2003–2006. National Health Statistics Reports, #10, 10 22, 2008.
40. Anthropometric Source Book, Volume 2 A Handbook of Anthropometric Data. NASA Reference Publication 1024, 1978.
41. Conti M Why is TOF PET reconstruction a more robust method in the presence of inconsistent data? Phys Med Biol 2011;56:155–168. [PubMed: 21119224]
42. Bal G, Panin V, Huff I, Michel C, Young J, Kehren F. Studying effects of missing data for clinical TOF PET. In: Conference Record of 2018 IEEE Nuclear Science Symposium and Medical Imaging Conference Piscataway, NJ: IEEE; 2018.
43. Yamaya T, Yoshida E, Inadama N, Nishikido F, Shibuya K, Higuchi M, Murayama H. A multiplex 'OpenPET' geometry to extend axial FOV without increasing the number of detectors. IEEE Trans Nucl Sci 2009;56:2644–2650.
44. Saloman A, Truhn D, Botnar R, Kiessling F, Schulz V. Sparse crystal setting and large axial FOV for integrated whole-body PET/MR. In: Chmeissani M, editor. Conference Record of 2011 IEEE Nuclear Science Symposium and Medical Imaging Conference Piscataway, NJ: IEEE; 2011.
45. Zhang J, Knopp MI, Knopp MV. Sparse detector configuration in SiPM digital photon counting PET: A feasibility study. Mol Imaging Biol 2019;21:447–453. [PubMed: 30094653]

46. Abi Akl M, Bouhali O, Toufique Y, Karp JS, Vandenberghe S. Monte Carlo sensitivity and count rate study of a long axial FOV PET scanner with patient adaptive rings. In: Conference Record of 2019 IEEE Nuclear Science Symposium and Medical Imaging Conference Piscataway, NJ: IEEE; 2019.
47. Efthimiou N, Whitehead AC, Stockhoff M, Thyssen C, Archibald SJ, Vandenberghe S. Preliminary investigation of the impact of axial ring splitting on image quality for the cost reduction of total-body PET. In: Conference Record of 2019 IEEE Nuclear Science Symposium and Medical Imaging Conference Piscataway, NJ: IEEE; 2019.
48. Zhang Z, Chen B, Perkins AE, Zio C-M, Sidky E, Manjeshwar RM, Pan X. Preliminary investigation of optimization-based image reconstruction for TOF PET with sparse configurations. In: Proc. SPIE 11072, 15th Intl Mtg on Fully Three-Dimensional Image Reconstruction in Radiology and Nuclear Medicine, Philadelphia, PA, 2019 DOI: 10.1117/12.2534846.
49. Zein SA, Karakatsanis NA, Issa M, Haj-Ali AA, Nehmeh SA. Physical performance of a long axial field-of-view PET scanner prototype with sparse rings configuration: A Monte Carlo simulation study. Med Phys (in press). DOI: 10.1002/mp.14046.
50. Joyce S, O'Connor OJ, Maher MM, McEntee MF. Strategies for dose reduction with specific clinical indications during computed tomography. Radiography 2020;26:S62–S68. [PubMed: 32682731]
51. Shan H, Padole A, Homayounieh F, Kruger U, Doda Khera R, Nitiwarangkul C, et al. Competitive performance of a modularized deep neural network compared to commercial algorithms for low-dose CT image reconstruction. Nature Machine Intelligence 2019;1:269.
52. Spencer BA, Schmall JP, Berg E, Omidvari N, Leung E, Deng Z, et al. Performance evaluation of the EXPLORER total-body PET/CT scanner based on NEMA NU-2 2018 standard with additional tests of extended geometry In: Conference Record of 2019 IEEE Nuclear Science Symposium and Medical Imaging Conference Piscataway, NJ: IEEE; 2019.
53. Badawi RD, Shi H, Hu P, Chen S, Xu T, Price PM, et al. First human imaging studies with the EXPLORER total-body PET scanner. J Nucl Med 2018;60:299–303.
54. Karp JS, Viswanath V, Geagan M, Muehllehner G, Pantel A, Parma M, et al. PennPET Explorer: Design and preliminary performance of a whole-body imager. J Nucl Med 2019;61:136–143. [PubMed: 31227573]
55. Pantel AR, Viswanath V, Daube-Witherspoon ME, Dubroff JG, Muehllehner G, Parma MJ, et al. PennPET Explorer: Human imaging on a whole-body imager. J Nucl Med 2019;61:144–151. [PubMed: 31562224]
56. Karp JS, Daube-Witherspoon ME, Hoffman EJ, Lewellen TK, Links JM, Wong W-H, Hichwa RD, Casey ME, Colsher JG, Hitchens RE, Muehllehner G, Stoub EW. Performance standards in positron emission tomography. J Nucl Med 1991;32:2342–2350. [PubMed: 1744726]
57. Daube-Witherspoon ME, Karp JS, Casey ME, DiFilippo FP, Hines H, Muehllehner G, Simcic V, Stearns CW, Aam L-E, Kohlmyer S, Sossi V. PET performance measurements using the NEMA NU 2–2001 standard. J Nucl Med 2002;43:1398–1409. [PubMed: 12368380]
58. Hudson HM, Larkin RS. Accelerated image reconstruction using ordered subsets of projection data. IEEE Trans Med Imaging 1994;13:601–609. [PubMed: 18218538]
59. Gong K, Berg E, Cherry SR, Qi JY. Machine learning in PET: From photon detection to quantitative image reconstruction. Proc IEEE 2020;108:51–68.
60. Moskal P, Rundel O, Alfs D, Bednarski T, Bialas P, Czerwin'ski E, et al. Time resolution of the plastic scintillator strips with matrix photomultiplier readout for J-PET tomograph. Phys Med Biol 2016;65:2025–2047.

Synopsis

This paper describes aspects of PET scanner design for long axial field-of-view systems and how these choices impact scanner performance.

Key Points

- Long axial field-of-view PET scanners offer the simultaneous advantage of greatly increased body coverage in a single bed position and much higher detection sensitivity.
- Long axial field-of-view PET scanners have been developed and demonstrate the performance possible with longer scanners while also highlighting the challenges associated with these systems.
- For clinical applications, the increased detection efficiency allows some combination of increased signal-to-noise ratio in the images, shorter acquisition times, or lower injected activity.
- For research applications, the dynamics of radiotracers across multiple organ systems or even the entire body is now possible.

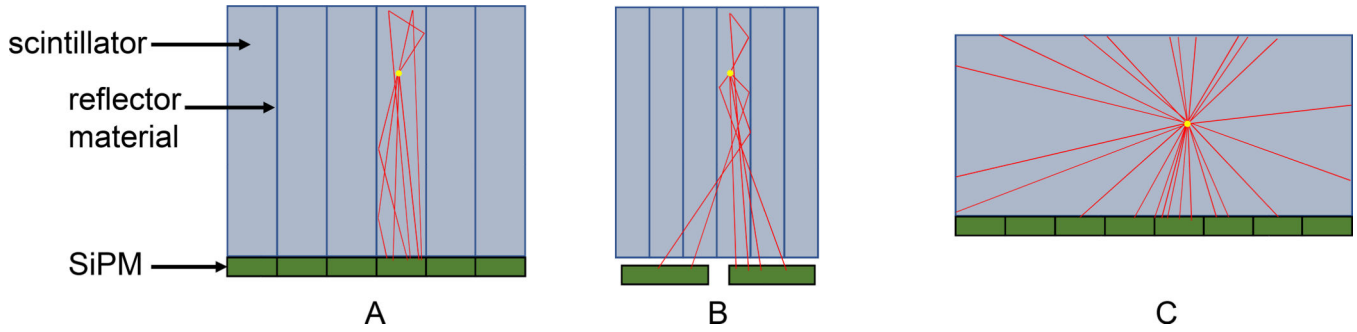

Figure 1.

Schematic cross-section through different types of PET detectors. a) Pixelated with 1:1 coupling; b) pixelated with light sharing using partial reflector coverage along length of crystals; c) monolithic detector. The red lines indicate sample scintillation light trajectories for a 511-keV photon interaction demonstrating the light distribution on the SiPMs reading out the scintillator.

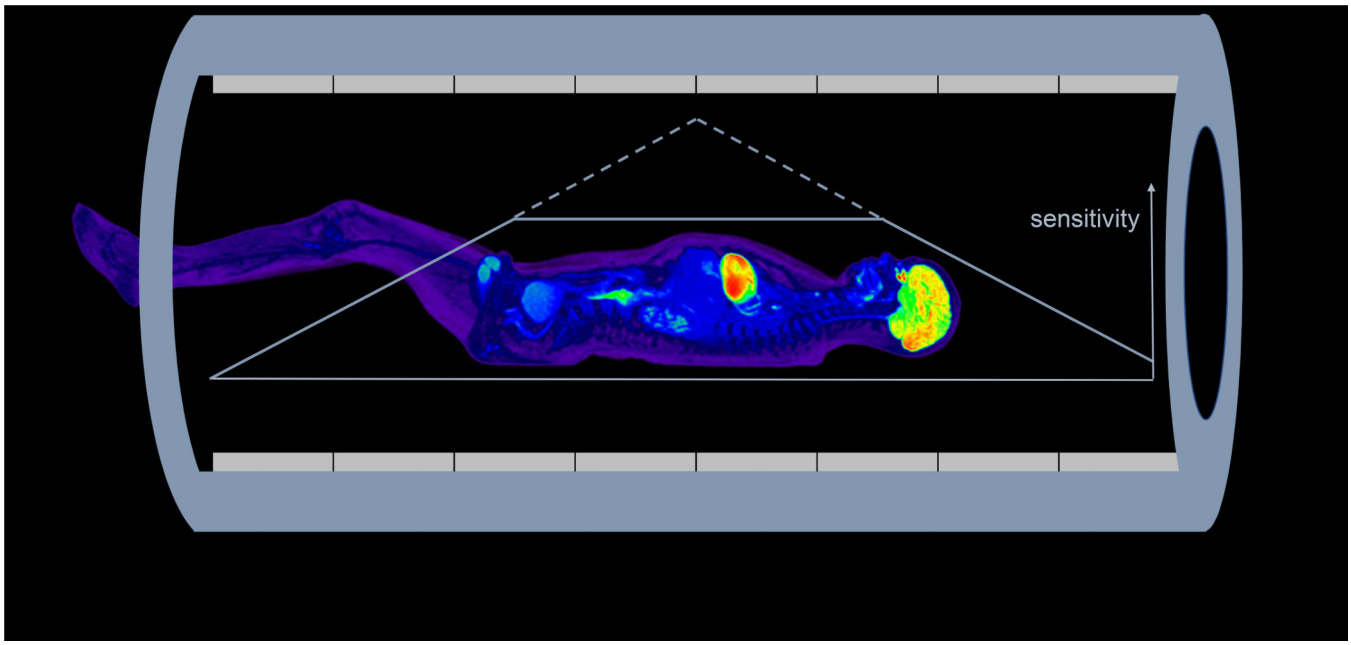

Figure 2.

Schematic showing geometric sensitivity to a point source as a function of axial location for a 2-m long scanner (dashed line) and after the axial acceptance angle is restricted to 57° (solid line). Profile is superimposed on the image of an average height human subject, demonstrating how a ~2-m length ensures very high and uniform sensitivity across all the major organs from brain to pelvis.

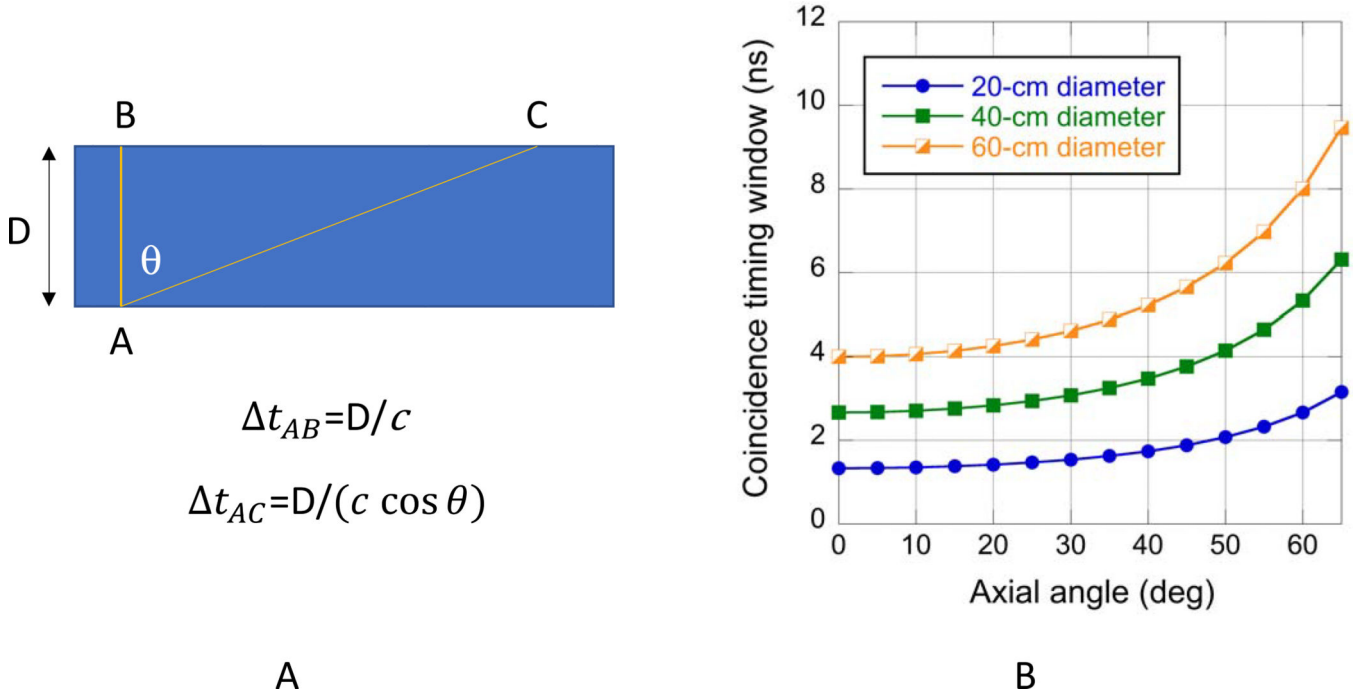

Figure 3.

a) Illustration of the time needed to capture all valid coincidences arising along a LOR as a function of axial acceptance angle, θ, and object diameter, D. b) Plot of the coincidence window as a function of angle for different sized objects. It is observed that for very steep angles, the coincidence timing window needed to measure all true coincidences along those LORs increases dramatically; however, these very oblique LORs are also highly attenuated, so few valid coincidences at these angles are actually detected.

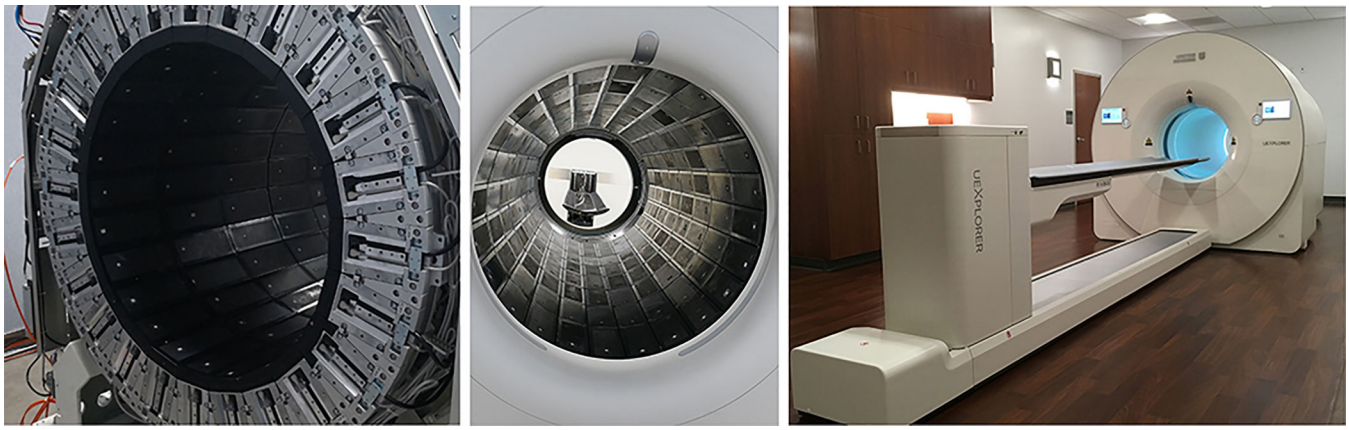

Figure 4.
Photographs of the uEXPLORER total-body PET/CT scanner during construction and after installation at UC Davis.

A

B

Figure 5.

a) Photograph of PennPET Explorer with 5 detector rings before cosmetic covers have been installed and cabling arrangement completed. An in-line Philips CT (with covers) is to the right of the PET system. The detector rings are mounted on rails and can be moved for maintenance; there is room for the 6th ring at the left end of the imager. b) Photograph of the back of the PennPET Explorer with a 10-cm diameter pipe phantom in place. The electronics for the 18 detector modules are seen behind the Plexiglas coverings.

Table 1.

Performance characteristics* of selected commercial SiPM-based TOF-PET scanners

	Philips Vereos[12]	Siemens Vision[13]	GE Discovery MI[18,14]	United Imaging uMI 550[19]	Canon Cartesian Prime[20]
Crystal & size (mm^3)	LYSO 3.86×3.86×19	LSO 3.2×3.2×20	LYSO 3.95×5.3×25	LYSO 2.76×2.76×16.3	Lu-based 4.2×4.2×20
Axial FOV (cm)	16.4	26.1	20 / 25	24	27
Sensitivity (70-cm line) (kcps/MBq)	5.7	16.4	13.7 / 20.8	10.2	13.5
TOF resolution	332 ps	210 ps	382 ps	372 ps	257 ps
Spatial resolution (@r=1 cm)	4.0 mm	3.5 mm	4.3 mm	2.9 mm	2.9 mm

* Performance specifications following NEMA standard[21].

Table 2.

Performance characteristics of long AFOV TOF-PET scanners

	uEXPLORER[52]	PennPET Explorer[54]
Crystal & size (mm^3)	LYSO 2.76×2.76×18.1	LYSO 3.86×3.86×19
Axial FOV (cm)	194	64 / 112 *
Sensitivity (70-cm line) (kcps/MBq)	174	54 / 83
Sensitivity (170-cm line) (kcps/MBq)	147	23 / 35
TOF resolution	509 ps	256 ps
Spatial resolution (@r=1 cm)	3 mm	4 mm

* Results are reported for the 3 / 5 ring configurations.